A Millimeter-Wave Integrated-Circuit Antenna Based on the Fresnel Zone Plate

Mark A. Gouker, *Student Member, IEEE* and Glenn S. Smith, *Fellow, IEEE*

Abstract—**A new type of millimeter-wave integrated-circuit antenna is investigated. The antenna is based on a quasi-optical design and consists of a Fresnel zone plate on one side of a dielectric substrate and a resonant strip dipole antenna at the focus of the zone plate on the opposite side of the substrate. The unique feature of this design is that all of the components are made using simple integrated-circuit fabrication techniques: thin film metal depositions on planar dielectric substrates. Another unusual feature of this design is the short focal length of the zone plate; the focal length/diameter (f/d) for the zone plates studied ranges from 0.1 to 0.5. The antennas described are for a frequency of 230 GHz (λ_o = 1.3 mm); however, the design is easily scaled to other millimeter-wave or submillimeter-wave frequencies. Measured results are reported for four different focal length zone plates. Moderate gains, above 20 dB, are obtained. A theory is developed which predicts the on-axis gain, beamwidth, and side lobe levels. Design graphs are given to aid in the selection of the geometrical parameters to achieve a desired gain from the integrated-circuit zone-plate antenna.**

I. Introduction

In SOME microwave and millimeter-wave systems, the simplicity of the design and the economy of the production can be greatly enhanced by constructing the antenna on the same substrate as the integrated circuitry. At microwave frequencies the microstrip patch antenna is commonly used for this purpose. However, as the frequency is increased into the millimeter-wave region, guided waves in the substrate start to make the microstrip patch antenna less efficient [1], [2]. This is true for microstrip antennas and for substrate-mounted antennas which do not have a ground plane on the side of the substrate opposite the antenna element.

This paper is concerned with substrate-mounted antennas for millimeter-wave frequencies. Two methods have been used to reduce the loss to guided waves in the substrate for these antennas. The first method employs a quasi-optical device placed on the opposite side of the substrate from the antenna [3]. The quasi-optical device reduces the loss to the guided waves by altering the boundary conditions (parallel-plane, dielectric-air interfaces) usually associated with the slab waveguide. A hemispherical lens was the first quasi-optical device used for this purpose [4], [5]. A bow-tie antenna was placed at the focal point of the lens on the opposite side of the substrate. Since then, a variety of antennas have been used with the hemispherical lens [6]–[8]. Recently a dielectric-filled paraboloidal reflector was investigated as a quasi-optical element [9]. The curved reflector was placed on the back side of the substrate, and the incident radiation focused onto the antenna element on the front side of the substrate, much as for a conventional paraboloidal reflector antenna. In the second method used to reduce the loss to guided waves in the substrate, the antenna is placed on a physically thin dielectric film (~ 1 μm) suspended from a semiconductor substrate [10], [11]. Since the film is also electrically thin, it does not strongly support the guided waves.

In this paper the quasi-optical approach is taken to reduce the loss to guided waves in the substrate. Unlike previous works, the design described here consists exclusively of planar elements. The novelty of this antenna is its ease of fabrication: it is constructed from planar dielectric substrates and thin-film metal depositions using conventional integrated-circuit processing.

II. Design

The antenna is composed of a Fresnel zone plate on one side of the substrate with a strip dipole antenna at the focal point of the zone plate on the opposite side of the substrate, Fig. 1. The main function of the zone plate is to form an antenna with substantially higher gain than that for the dipole alone. In addition, the zone plate also reduces the energy loss to guided waves in the substrate by altering the boundary conditions of the dielectric slab waveguide. Only now it is the nonperiodic boundary condition formed by the metal zone-plate rings that causes the alteration.

Zone-plate antennas previously have been used in the microwave [12] and the millimeter-wave regions [13], but not in a form suitable for incorporation into an integrated circuit. The antenna reported here is easily incorporated into an integrated circuit. The dipole or other feed element is placed on the same side of the substrate as the

Manuscript received July 22, 1991; revised December 30, 1991. This work was supported in part by the Georgia Tech Research Institute under Projects E904-017 and E904-034 and by the Joint Services Electronics Program under Contracts DAAL03-87-K-0059 and DAAL-03-90-C-0004.

M. A. Gouker was with the School of Electrical Engineering, Georgia Institute of Technology, Atlanta, GA 30332-0250. He is presently with the Lincoln Laboratory, Massachusetts Institute of Technology, Lexington, MA 02173-9108.

G. S. Smith is with the School of Electrical Engineering, Georgia Institute of Technology, Atlanta, GA 30332-0250.

IEEE Log Number 9107024.

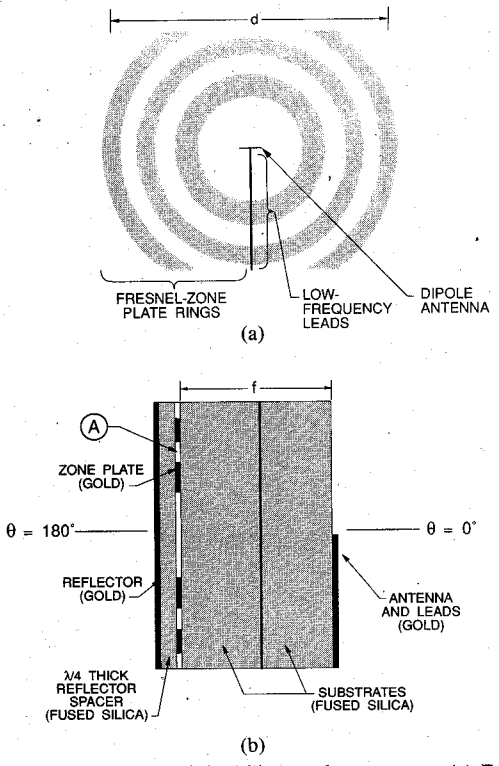

Fig. 1. Schematic drawing of the IC zone-plate antenna. (a) Front view. (b) Side view.

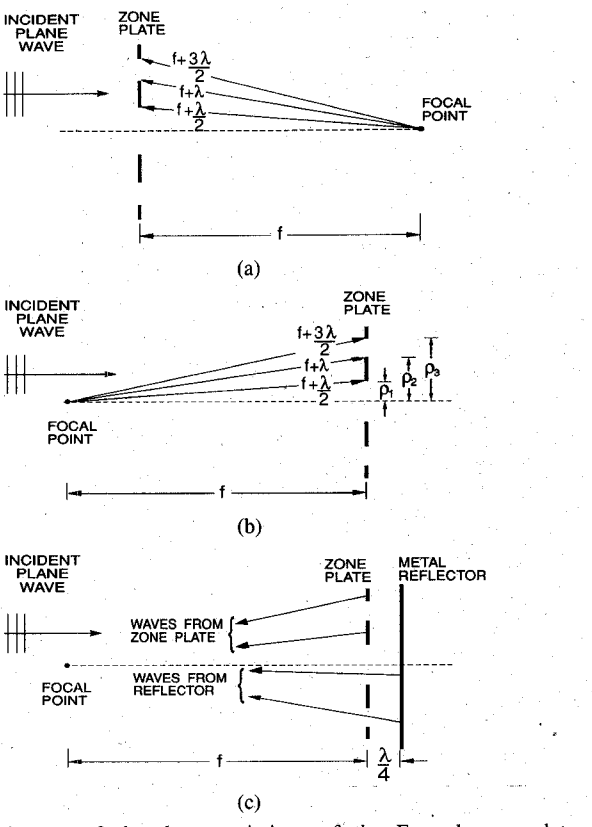

Fig. 2. Diagram of the three variations of the Fresnel zone plate: (a) Transmission Fresnel zone plate. (b) Reflection Fresnel zone plate. (c) Folded Fresnel zone plate.

integrated circuitry, and the zone plate is placed on the opposite, often unused, side.

The operation of the Fresnel zone plate used in this work can be understood with the aid of the illustrations presented in Fig. 2. The *transmission Fresnel zone plate*, shown in Fig. 2(a), concentrates energy at a focal point by blocking the portions of the incident wave that would add destructively at the focal point. In the most basic treatment of the zone plate, the incident wave is replaced by point sources in the open regions of the zone plate. The geometry of the open and opaque regions is chosen so that the path lengths for waves traveling from the point sources to the focal point result in constructive interference (relative phase between 0 and π). The cylindrical symmetry about the axis normal to the zone plate gives the structure its characteristic clear and opaque rings, Fig. 1(a). The zone plate can also be used in a reflection configuration if the opaque regions are replaced by reflecting surfaces, as in Fig. 2(b). This is called a *reflection Fresnel zone plate*. The portion of the incident wave that passes through the open regions of the reflection zone plate can be made to add constructively at the focal point by placing a planar reflector behind the zone plate, Fig. 2(c). The $\lambda/4$ spacing between the reflector and the zone plate results in a round-trip phase change of π; therefore, this portion of the incident wave also arrives at the focal point with a relative phase between 0 and π. This configuration is called the *folded Fresnel zone plate*, and it is the configuration used for the antennas in this work, Fig. 1(b).

The radii of the zone-plate rings are determined from strictly geometric considerations, with the nth radius, ρ_n, given by

$$\rho_n = \sqrt{nf\lambda + \left(\frac{n\lambda}{2}\right)^2}, \tag{1}$$

where f is the focal length of the zone plate (the substrate thickness) and λ is the wavelength in the substrate. The first three radii are indicated in Fig. 2(b). The rings for the IC zone-plate antennas in this work were designed using the simple geometric considerations presented above (1), and these were found to yield good results. However, other considerations are possible, and these will be discussed later in this paper.

III. Theory

A simple analysis was developed for the integrated-circuit zone-plate antenna; it is based on the plane wave spectrum for an antenna near the interface separating two dielectric half-spaces. The methodology and notation used are presented in reference [14]. In this approach the field radiated from an isolated antenna is represented by a spectrum of plane waves that propagate away from the antenna in all directions. The amplitude of these plane waves is given by the spectral density function which is determined from the current in the antenna. The advantage of this

approach for the IC zone-plate antenna is that the passage of the individual plane waves through the interfaces of the substrate is easily handled using the Fresnel reflection and transmission coefficients.

The analysis for the IC zone-plate antenna is outlined in the flow chart shown in Fig. 3. The dipole is assumed to be infinitesimally small and located on the surface of the substrate. The far-zone field of the dipole, in the air and in the substrate, is found using the plane wave spectrum [14]. The current in the zone-plate rings and reflector is then determined using the field of the dipole in the substrate with the physical optics approximation. The spectral density function for this current is then calculated. The individual plane waves in this spectrum are transmitted through the substrate, and the far-zone field of the zone-plate rings and reflector is determined in the air. Finally, the field of the dipole is added to the field of the zone-plate rings and reflector to obtain the total far-zone field in the air.

An approximation is introduced to handle the reflector placed behind the zone-plate in the folded zone-plate configuration, Fig. 2(c). The reflector is modeled by placing fictitious, perfectly conducting rings between the actual perfectly conducting rings of the zone plate. A phase shift of π is added to the physical optics current on the fictitious rings to account for the additional $\lambda/2$ path length for a wave traveling from the plane of the zone plate to the reflector and back.

The coordinate systems used in the IC zone-plate antenna analysis are given in Fig. 4. The dipole is at the origin of the unprimed coordinate system, and the zone plate is centered at the origin of the primed coordinate system. The coordinates of the observation point in the air are given in the unprimed system (r, θ, ϕ), and the coordinates of a point on the zone plate (used in the calculation of the physical optics current) are also given in the unprimed system but are denoted by the subscript p (r_p, θ_p, ϕ_p).

The expressions for the far-zone electric field of an infinitesimal dipole (current in the y direction) on the surface of a dielectric half-space are given in [14]: in the substrate, region 1,

$$\vec{E}_1^r = \omega^2 \mu_o p \{-\hat{\theta} \sin \phi_p |\cos \theta_p| [1 - R_\parallel(K_{S1})] + \hat{\phi} \cos \phi_p [1 + R_\perp(K_{S1})]\} \frac{e^{-jk_1 r_p}}{4\pi r_p}, \tag{2a}$$

and in the air, region 2,

$$\vec{E}_2^r = \omega^2 \mu_o p k_{21} |\cos \theta| \left\{\hat{\theta} \sin \phi T_\parallel(K_{S2}) + \hat{\phi} \frac{\cos \phi T_\perp(K_{S2})}{\sqrt{1 - k_{21}^2 \sin^2 \theta}}\right\} \frac{e^{-jk_2 r}}{4\pi r}. \tag{2b}$$

Here $p = -jI\Delta l/\omega$ is the moment of the electrically short dipole with the current I and the length Δl,

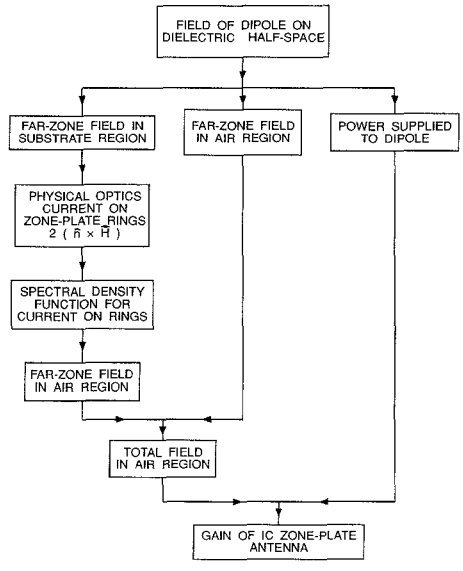

Fig. 3. Flow chart for the IC zone-plate antenna analysis.

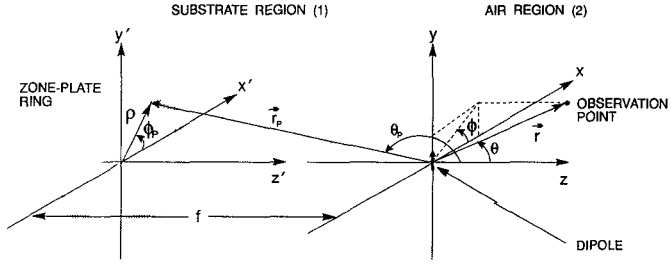

Fig. 4. Coordinate systems for the IC zone-plate antenna analysis.

$$K_{Si} = k_i \sin \theta, \qquad i = 1, 2 \tag{3a}$$

and

$$k_{21} = 1/k_{12} \equiv k_2/k_1, \tag{3b}$$

where k is the wave number. $R_{\parallel,\perp}(K_{Si})$ and $T_{\parallel,\perp}(K_{Si})$ are the Fresnel reflection and transmission coefficients, respectively, evaluated at K_{S1} or K_{S2} depending on the region of observation:

$$R_\parallel(K_{S1}) = \frac{k_{21}^2 |\cos \theta_p| - \sqrt{k_{21}^2 - \sin^2 \theta_p}}{k_{21}^2 |\cos \theta_p| + \sqrt{k_{21}^2 - \sin^2 \theta_p}}, \tag{4a}$$

$$R_\perp(K_{S1}) = \frac{|\cos \theta_p| - \sqrt{k_{21}^2 - \sin^2 \theta_p}}{|\cos \theta_p| + \sqrt{k_{21}^2 - \sin^2 \theta_p}}, \tag{4b}$$

$$T_\parallel(K_{S2}) = \frac{2k_{12}\sqrt{k_{12}^2 - \sin^2 \theta}}{k_{12}^2 |\cos \theta| + \sqrt{k_{12}^2 - \sin^2 \theta}}, \tag{4c}$$

$$T_\perp(K_{S2}) = \frac{2\sqrt{k_{12}^2 - \sin^2 \theta}}{|\cos \theta| + \sqrt{k_{12}^2 - \sin^2 \theta}}. \tag{4d}$$

The expression for the field in the substrate (region 1) is used to calculate the physical optics current, $\vec{K}_e$ =

$2(\hat{n} \times \vec{H}_1^r)$, on the zone-plate rings. The x' and y' components of this surface current are

$$K_{e,x'} = -\frac{2}{\zeta_1}\omega^2\mu_o p\frac{e^{-jk_1 r_p}}{4\pi r_p}|\cos\theta_p|\cos\phi_p \cdot \sin\phi_p[R_\parallel(K_{S1}) + R_\perp(K_{S1})], \quad (5a)$$

and

$$K_{e,y'} = \frac{2}{\zeta_1}\omega^2\mu_o p\frac{e^{-jk_1 r_p}}{4\pi r_p}|\cos\theta_p|\{[1 - R_\parallel(K_{S1})] \cdot \sin^2\phi_p + [1 + R_\perp(K_{S1})]\cos^2\phi_p\}. \quad (5b)$$

The spectral density function for the current on the zone-plate rings and fictitious rings is determined from equation (37) in [14]. The variables of integration over the rings are changed from x' and y' to ρ and ϕ_p, and the following substitutions are made

$$r_p = \sqrt{f^2 + \rho^2}, \quad (6a)$$

and

$$|\cos\theta_p| = \frac{f}{\sqrt{f^2 + \rho^2}}, \quad (6b)$$

where f is the focal length, which is the substrate thickness, and ρ is the radial distance on the plane of the zone plate. The integration with respect to ϕ_p can be evaluated in closed form if the observation point in the air region is restricted to the two principal planes. The first principal plane, $\phi = \pi/2$, (see Fig. 4) is referred to as the E-plane (with respect to the dipole), and the second principal plane, $\phi = 0$, is referred to as the H-plane. The ρ integral must be performed numerically. The loss in the substrate is added only in the wave number when it occurs in the exponential terms, $e^{-jk_1 r}(k_1 = \beta_1 - j\alpha_1)$. The far-zone electric field produced in the air by the zone-plate rings and fictitious rings is determined using equation (21) in [14]: for the E-plane

$$\vec{E}_2^r(r, \theta, \phi = \pi/2) = -\hat{\theta}\frac{j}{2}\omega^2\mu_o p\frac{e^{-jk_2 r}}{4\pi r}\exp[-jk_1 f\sqrt{1 - k_{21}^2\sin^2\theta}] \cdot k_2|\cos\theta|\,T_\parallel(K_{S2})\sum_{n=1}^{N_{HZ}}(-1)^n\int_{\rho_{n-1}}^{\rho_n} \cdot \frac{\exp(-jk_1\sqrt{f^2 + \rho^2})}{[f^2 + \rho^2]} f\rho\{[1 - R_\parallel(K_{S1})] \cdot [J_0(k_2\rho\sin\theta) - J_2(k_2\rho\sin\theta)] + [1 + R_\perp(K_{S2})][J_0(k_2\rho\sin\theta) + J_2(k_2\rho\sin\theta)]\}\,d\rho, \quad (7a)$$

and for the H-plane

$$\vec{E}_2^r(r, \theta, \phi = 0) = -\hat{\phi}\frac{j}{2\sqrt{1 - k_{21}^2\sin^2\theta}}\omega^2\mu_o p\frac{e^{-jk_2 r}}{4\pi r} \cdot \exp[-jk_1 f\sqrt{1 - k_{21}^2\sin^2\theta}]k_2|\cos\theta|\,T_\perp(K_{S2}) \cdot \sum_{n=1}^{N_{HZ}}(-1)^n\int_{\rho_{n-1}}^{\rho_n}\frac{\exp(-jk_1\sqrt{f^2 + \rho^2})}{[f^2 + \rho^2]} f\rho \cdot \{[1 - R_\parallel(K_{S1})][J_0(k_2\rho\sin\theta) + J_2(k_2\rho\sin\theta)] + [1 + R_\perp(K_{S2})][J_0(k_2\rho\sin\theta) - J_2(k_2\rho\sin\theta)]\}\,d\rho. \quad (7b)$$

In these expressions J_n is the Bessel function of the first kind and order n, N_{HZ} is the total number of half zones, where a half zone is either an actual zone-plate ring or a fictitious zone-plate ring, and ρ_{n-1} and ρ_n are given by (1). The total electric field in the air region is the sum of the field of the zone-plate rings (7a or 7b) and the field of the dipole (2b).

To calculate the gain of the zone-plate antenna, the power supplied to the dipole is needed. This is taken to be the power supplied to a dipole on the surface of a dielectric half-space and determined using equations (36), (45a) and (50a) in [14]:

$$P_{\text{in}} = (\omega^2\mu_o p)^2\frac{1}{16\pi\zeta_1}\left(4/3 - \frac{1}{k_1}\int_0^{k_{21}}\gamma_1(\xi)\left[R_\parallel(\xi) - \left(\frac{k_1}{\gamma_1(\xi)}\right)^2 R_\perp(\xi)\right]\xi\,d\xi, - \frac{1}{k_1}\int_{k_{21}}^{1}\gamma_1(\xi)\left\{\text{Re}\,[R_\parallel(\xi)] - \left(\frac{k_1}{\gamma_1(\xi)}\right)^2 \cdot \text{Re}\,[R_\perp(\xi)]\right\}\xi\,d\xi\right), \quad (8)$$

where

$$R_\parallel(\xi) = [k_2^2\gamma_1(\xi) - k_1^2\gamma_2(\xi)]/[k_2^2\gamma_1(\xi) + k_1^2\gamma_2(\xi)], \quad (9a)$$

$$R_\perp(\xi) = [\gamma_1(\xi) - \gamma_2(\xi)]/[\gamma_1(\xi) + \gamma_2(\xi)], \quad (9b)$$

with

$$\gamma_1(\xi) = k_1\sqrt{1 - \xi^2}, \quad (9c)$$

$$\gamma_2(\xi) = k_1\sqrt{k_{21}^2 - \xi^2}. \quad (9d)$$

Finally, the gain of the zone-plate antenna is calculated from

$$G(\theta, \phi) = \frac{4\pi r^2\hat{r} \cdot \text{Re}\,[\vec{S}_c^r(r, \theta, \phi)]}{P_{\text{in}}}, \quad (10)$$

where $\vec{S}_c^r$ is the complex Poynting vector in the far zone.

IV. Fabrication and Measurements

All of the antennas measured in this work were designed for the frequency 230 GHz (λ_o = 1.3 mm). The zone plate, dipole structure, and reflector were fabricated on separate substrates and combined to form the total IC zone-plate antenna, as indicated in Fig. 1. All substrates were fused silica (Corning Glass Works, material code 7940). The dipole structure, shown in the photograph in Fig. 5, consists of four elements: a resonant dipole, a bismuth bolometer, an interdigitated capacitor, and low-frequency leads. The resonant dipole antenna receives the energy reflected from the zone plate, and the bismuth bolometer at the terminals of the dipole detects this energy. The interdigitated capacitor acts as a short circuit at the millimeter-wave frequency, thus preventing signals induced in the leads from reaching the detector. The unique U-shaped bolometer prevents the capacitor from also short circuiting the terminals of the dipole. At the millimeter-wave frequency, the terminals of the dipole see two bolometers in parallel: the direct path between the terminals and the path through the capacitor. The last element in the dipole structure is the low-frequency leads which carry the detected signal to the edge of the substrate for transmission to the external instrumentation.

Theoretical results for a dipole on the surface of a dielectric half space were used to determine the resonant length and resistance at resonance for the strip dipole [15]. The bolometer was then designed to have a resistance which roughly matched the resistance at resonance of the dipole.

The dipole structure was made in a three step process. First, the dipole, the interdigitated capacitor, and low-frequency leads were etched from a 150 Å chromium and 850 Å gold metallization layer. Second, the bismuth bolometer was formed by the lift-off process of a 3500 Å metallization. Third, the dipole, the interdigitated capacitor, and low-frequency leads were electroplated with gold to a total thickness between 1.0 and 1.5 μm. The electroplating step ensured that the dipole was several skin depths thick, and the added gold reduced the resistance of the leads that extend to the edge of the substrate. The zone plates were made with the same technique. The complete details of the design, the construction, and the experimental procedures are available elsewhere [16].

The *E*- and *H*-plane field patterns and the gains of the IC zone-plate antennas were measured on a specially constructed elevation-over-azimuth antenna range. The power transmitted from the source in the antenna range and the power received by the IC zone-plate antenna were measured at angular intervals of one degree, and the gain of the IC zone-plate antenna was calculated from the Friis transmission formula.

Four different zone-plate antennas were investigated. All had a nominal diameter of 21 mm but different focal lengths: $f/\lambda \approx 3$, 6, 9 and 15, with corresponding $f/d \approx 0.1$, 0.2, 0.3 and 0.5. In addition, a series of three measurements was made to investigate the contributions of the various elements that make up the zone-plate antenna. First, the dipole antenna on the substrate was measured alone; second, the combination of the dipole with the zone plate was measured, and third, the full IC zone-plate antenna (dipole, zone plate, spacer and reflector) was measured.

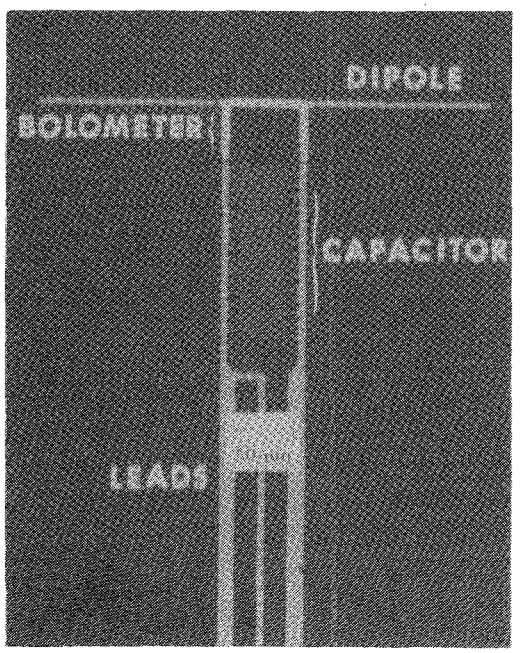

Fig. 5. Photograph of the dipole region of the IC zone-plate antenna.

The power patterns for the dipole alone on a substrate with a thickness of 1.54 λ are shown in Fig. 6. The theoretical curve in this figure is based on the electric field strength on the surface of the substrate calculated from the Fresnel reflection and transmission coefficients for a dielectric sheet. The magnitude of the theoretical gain has been normalized to the average of the measured on-axis gains. The good agreement between the measured and theoretical results confirms the validity of the measurement technique and the operation of the antenna range. Results for dipole antennas alone on other thicknesses of the substrate are presented elsewhere and show equally good agreement [16], [17].

The power patterns for the dipole and the Fresnel zone plate, without reflector or spacer, are shown for the zone plate with $f/d = 0.29$ and $f/\lambda = 9.0$ in Fig. 7. This figure shows that the zone plate can be used in both the reflection ($\theta = 0°$) and the transmission ($\theta = 180°$) configurations, as indicated earlier in Fig. 2. The on-axis gains for the reflection and transmission configurations are 22.6 dB and 20.7 dB, respectively. The difference in the gains for these two configurations is discussed in more detail below. The power patterns for the fully assembled IC zone-plate antenna, which includes the spacer and reflector, are shown in Fig. 8. The on-axis gain for this configuration is 25.6 dB, about 3 dB above that for the reflection zone plate and 5 dB above that for the transmission zone plate.

The difference between the gains of the reflection and transmission zone plates prompted another series of measurements to investigate the contribution of the reflections

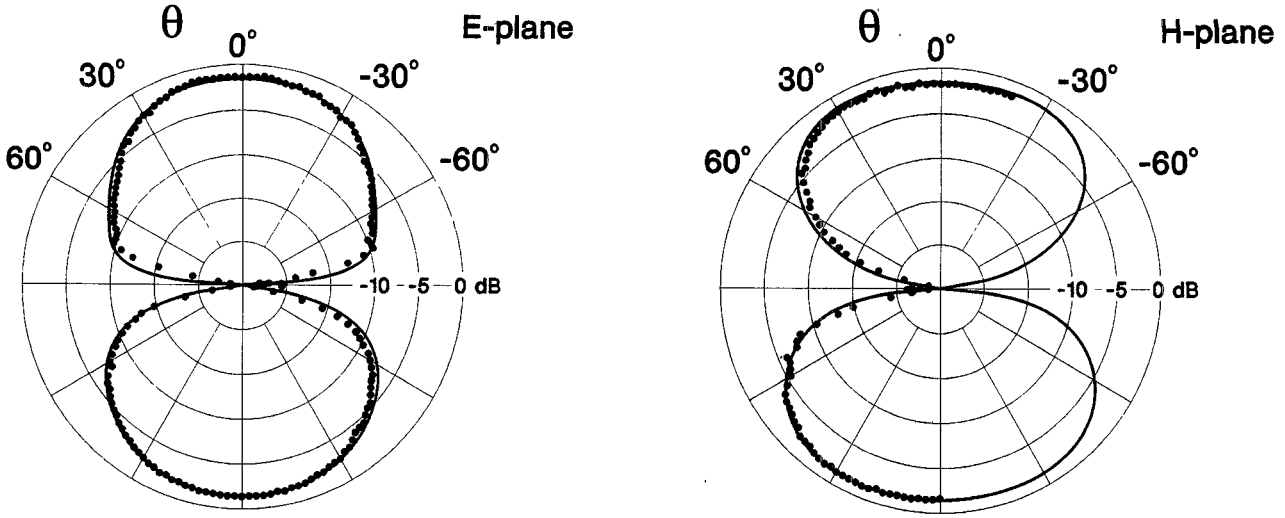

Fig. 6. Power patterns for the dipole, alone, on a fused silica substrate with a thickness of 1.5λ:—theory • measured.

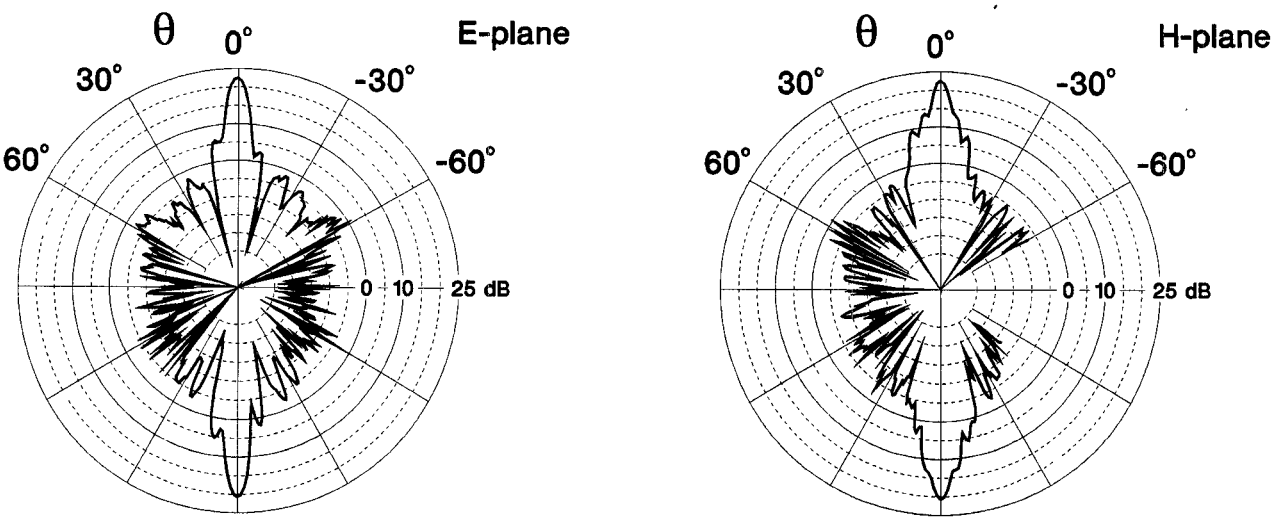

Fig. 7. Power patterns for the dipole and zone plate without reflector, $f/d = 0.29, f/\lambda = 9.0$.

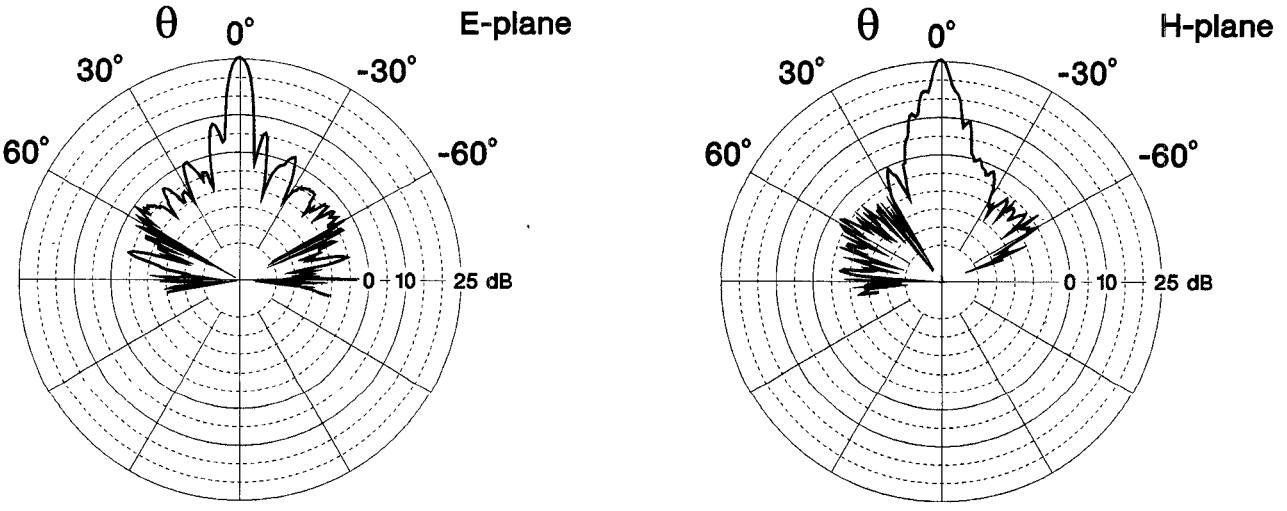

Fig. 8. Power patterns for the dipole with zone plate, spacer and reflector: the fully assembled integrated-circuit zone-plate antenna, $f/d = 0.29, f/\lambda = 9.0$.

from the dielectric-air interface at the plane of the zone plate, indicated by A in Fig. 1(b). The three curves in Fig. 9 are for the wave incident from the dipole side of the substrate ($\theta = 0°$), i.e., the reflection configuration. The curve with the lowest on-axis gain (20.6 dB) was made with a quarter-wave dielectric matching layer (Dupont, Teflon FEP) behind the zone plate. With the matching layer present, only one set of zone plate rings, the metal rings, reflects energy back to the dipole. The curve with the intermediate on-axis gain (22.6 dB) was made with nothing behind the zone plate. In this case there is a contribution from both sets of rings. The metal rings contribute to the gain as in the first case, but now the reflection from the dielectric-air interface, the open rings, also contributes to the gain. Note that there is a π phase difference between the reflection from the metal rings and the reflection from the open rings (dielectric-air interface) so that both reflected waves add in phase at the focal point of the zone plate. The curve with the highest on-axis gain (26.6 dB) is for the zone plate with the $\lambda/4$ spacer and reflector.

The measured results for the four fully configured IC zone-plate antennas with different focal lengths are summarized in Table I. The gain is maximum (25.2 dB) for the antenna with $f/\lambda = 9.0$. Attenuation in the substrate decreases the gain for the antenna with the longer focal length, $f/\lambda = 15$; for shorter focal lengths, the gain decreases with a corresponding increase in the beamwidth.

In Figs. 10 and 11, measured power patterns are compared to those calculated from the theory presented in the previous section for the antennas with $f/\lambda = 15$ and $f/\lambda = 9.0$, respectively. The measured and theoretical results are equated at one point for these graphs (0 dB at 0°); however, the actual measured and theoretical on-axis gains are indicated in the upper left-hand corner of each graph. The predicted on-axis gain, beamwidth and side lobe levels compare very well with the measured results for the these IC zone-plate antennas, even though the theory contains several assumptions, e.g., an infinitesimal dipole. The good agreement between the theoretical and measured gains indicates that guided waves in the substrate are not decreasing the efficiency of these antennas. This is probably due to the aforementioned nonperiodic boundary condition that the zone plate produces at the surface of the substrate.

The theory was found not to predict the measured results as well for the antennas with the shorter focal lengths: $f/\lambda = 6.0$ and $f/\lambda = 3.0$. The predicted beamwidths are smaller while the predicted gains are larger than the measured values. The failure of the theory for the extremely short focal length zone plates is thought to be caused by two effects. First, the width of the zone-plate rings decreases with decreasing focal length making the physical optics appoximation less valid for the current in the rings. Second, the substrate thickness decreases with decreasing focal length. This intensifies the effects of multiple reflections in the substrate of the fields radiated by the zone plate and reflector. These mulitple reflections

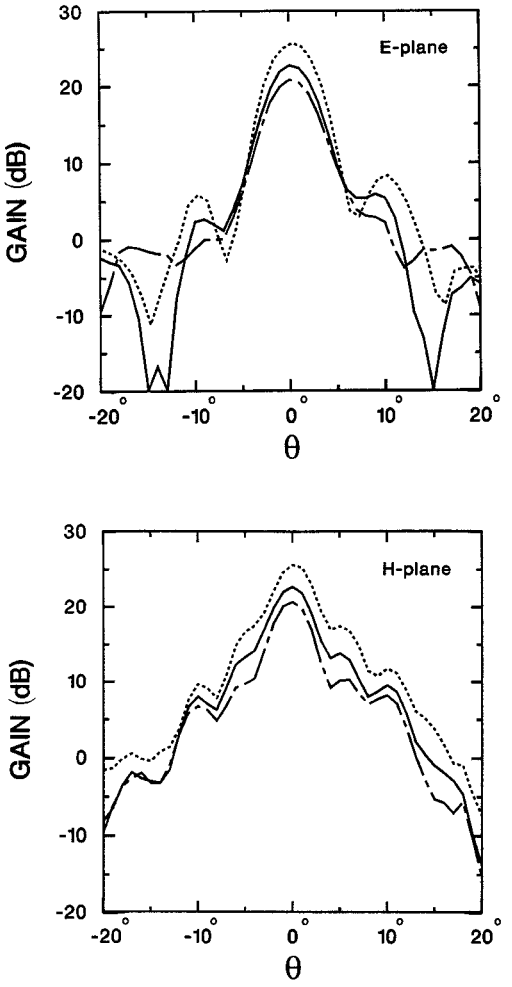

Fig. 9. Power patterns showing the contribution of the dielectric-air interface:— — — dielectric matching layer behind zone plate, ——zone plate with nothing behind,----zone plate with $\lambda/4$ spacer and reflector, $f/d = 0.29$, $f/\lambda = 9.0$.

TABLE I
MEASURED ON-AXIS GAINS AND BEAMWIDTHS OF IC ZONE-PLATE ANTENNAS

Focal Length		Diameter					Beamwidth (FWHM)	
mm	f/λ	mm	d/λ	Half Zones	f/d	Gain dB	E Plane	H Plane
2.0	3.01	20.87	31.46	26	0.096	16.5	14.9°	23.2°
4.0	6.03	21.13	31.85	22	0.19	21.3	7.1°	7.1°
6.0	9.04	20.72	31.28	18	0.29	25.2	4.5°	4.0°
10.0	15.07	21.40	32.26	14	0.47	23.3	4.2°	3.0°

modify the current distribution on the zone plate and reflector and are not taken into account in the present theory.

A design graph for the IC zone-plate antenna is shown in Fig. 12. This graph should be useful for designing other IC zone-plate antennas on substrates with a relative permittivity of $\epsilon_r = 3.8$ (fused silica). Lossless substrate material is assumed, since most substrates of practical interest are low loss. The gain of the IC zone-plate antenna is

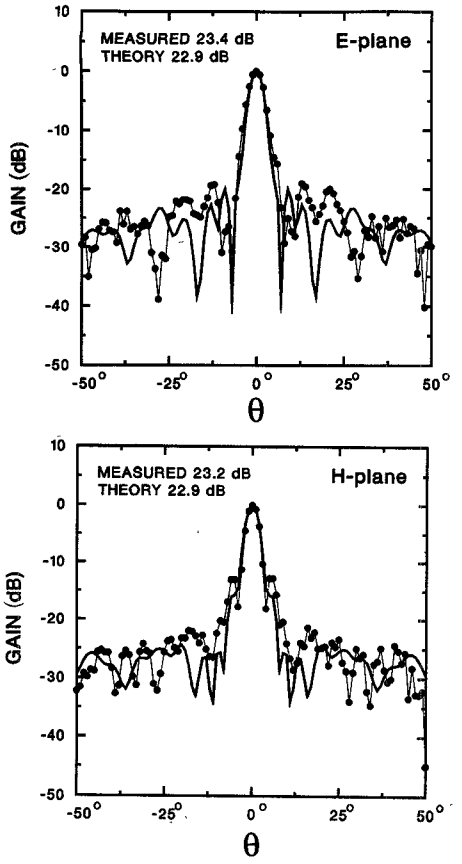

Fig. 10. Power patterns for the IC zone-plate antenna with $f/\lambda = 15$ and $f/d = 0.47$:——— Theory, •—•—• measured.

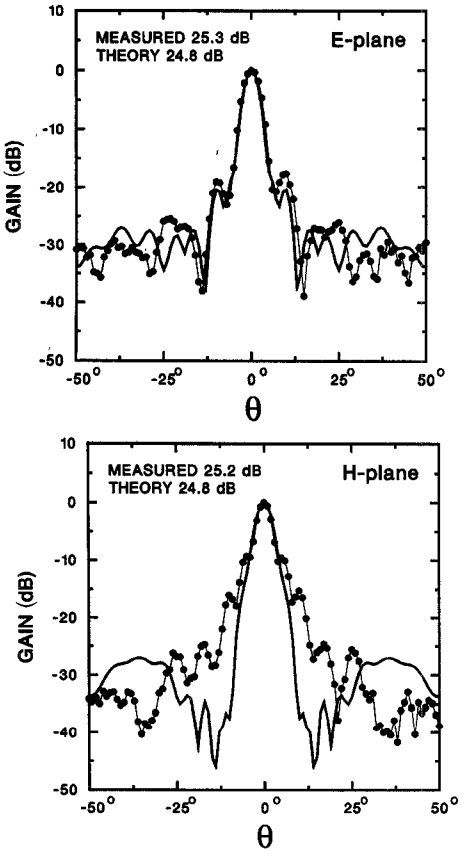

Fig. 11. Power patterns for the IC zone-plate antenna with $f/\lambda = 9.0$ and $f/d = 0.29$:——— theory, •—•—• measured.

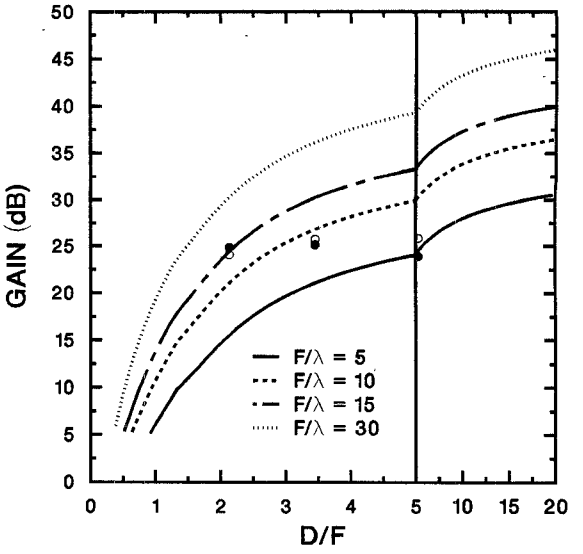

Fig. 12. Design graph for the IC zone-plate antenna on lossless substrate of relative permittivity $\epsilon_r = 3.8$: ○ theoretical points, • measured points.

plotted versus the diameter over the focal length, d/f. Notice that the horizontal scale has been compressed for values of d/f greater than 5. Each curve is for a constant focal length f/λ.

The points marked on the graph are a comparison between the measured and predicted gains for the antennas in this work: $f/\lambda = 15$, 9.0 and 6.0. The open circles are the theoretical gains, and the solid circles are the measured gains for these antennas with a minor correction factor added to remove the substrate loss.

V. Discussion

The discussion in this section centers on the phase of the field produced directly in the substrate by the transmitting dipole and the effects of this phase on the design of the zone plate placed on the opposite side of the substrate. The equation, (1), used to determine the radii of the zone-plate rings is based on strictly geometric considerations: the phase of the field on the zone plate is determined as if the transmitting dipole were in an infinite dielectric medium. However, it is seen from (2a) that the field on the zone plate from a transmitting dipole on the interface separating two dielectric half spaces is more complicated.

In Fig. 13 the electric field on the zone plate with reflector ($f/\lambda = 15$) is graphed for two cases: a dipole on the air-dielectric (substrate) interface, the solid line, and a dipole in an infinite dielectric (substrate) medium, the dashed line. The field on the axis parallel to the dipole (the y′-axis in Fig. 4) and the field on the axis perpendicular to the dipole (the x′-axis in Fig. 4) are presented. Note, the phase change associated with modeling the reflector by the fictitious perfectly conducting rings is included in the graphs.

The difference between these two cases is due solely to the portion of the field radiated from the dipole on the air-dielectric interface that is reflected at this interface. One

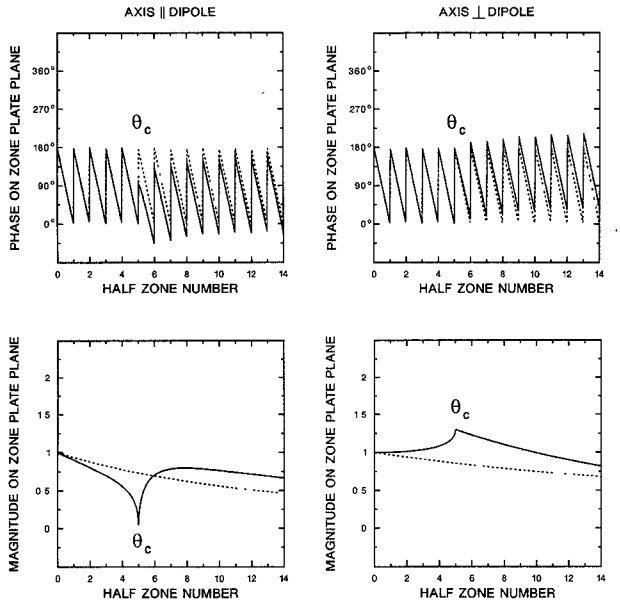

Fig. 13. Phase and magnitude of dipole field on zone plate, $f/\lambda = 15$, $f/d = 0.49$, ——dipole on air-dielectric interface,---dipole in an infinite dielectric medium.

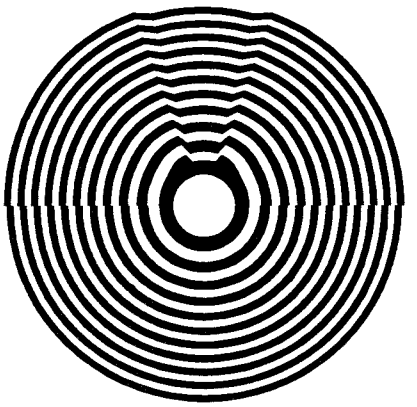

Fig. 14. Top half: zone-plate rings for a dipole on an air-dielectric interface. Bottom half: zone-plate rings for a dipole in an infinite dielectric medium.

can think of the dipole as being slightly inside the substrate, then there is a reflection of the dipole field from the surface of the substrate. Along both zone-plate axes, the phase of the field for angles less than the critical angle, θ_c, is the same for the two cases. This is because the phase of the reflection coefficient is zero for *angles less than the critical angle*. However, for the portion of the field that is reflected from this interface at *angles greater than the critical angle*, the reflection coefficient has a nonzero phase and a magnitude of one. Thus, when the reflected wave is added to the wave radiated directly by the dipole, the phase of the field on the zone plate differs from the phase of the field radiated by the dipole in the infinite dielectric medium. There is only a minor difference in the phases of the fields for the two cases; therefore, zone-plates designed assuming the dipole is in an infinite medium, as in this paper, work well for the IC zone-plate antenna on substrates with $\epsilon_r = 3.8$. However, the phase distortion of the field on the zone plate is more pronounced for higher permittivity substrates, and an alternate method for determining the zone-plate rings is worth consideration.

From the results presented in Fig. 13, it appears that the *width* and the *shape* of the zone-plate rings could be adjusted to increase the gain for the IC zone-plate antenna. The boundaries of the half-zones could be determined by drawing contours where the phase of the field changes by π from the phase of the previous half-zone boundary. This is a straightforward procedure along the axes parallel and perpendicular to the dipole where the field is linearly polarized, Fig. 13. The field, however, is elliptically polarized on the other regions of the zone plate, and some thought must be given as to how the half-zone boundaries are to be determined.

One of these zone plates was designed for a substrate with $\epsilon_r = 3.8$ and the focal length $f/\lambda = 6.0$ by ignoring the component of the current on the zone plate perpendicular to the dipole, $K_{e,x'}$. This is a reasonable approximation since this component of the current does not contribute (integrates to zero) to the spectral density function for the zone plate and reflector when the observation point is in the E-plane or H-plane ($\phi = \pi/2$ or 0). The ring structure for this zone plate is compared to that for a standard zone plate in Fig. 14. The distorted rings in the top half of the figure are for the dipole on the air-dielectric interface, and the circular rings in the bottom half of the figure are for a dipole in an infinite dielectric medium (the standard zone plate).

The distorted zone-plate design should enhance the performance of the IC zone-plate antenna. Antennas on high permittivity substrates should benefit more from this modification than antennas on low permittivity substrates, since the distortion of the phase of the field on the zone plate is greater for antennas on high permittivity substrates.

VI. Conclusion

A moderate gain, easily constructed, millimeter-wave integrated-circuit antenna based on the Fresnel zone plate was developed. The gain and beamwidth of the antenna can be varied by adjusting the diameter and focal length of the zone plate, f/d and f/λ; this gives the designer some latitude in fitting an antenna to a particular system's requirements. A theory was developed which accurately predicts the on-axis gain, beamwidth and side lobe levels for antennas with zone-plate focal lengths greater than 8–9λ. Graphs were presented to aid in the design of other IC zone-plate antennas.

The performance of the IC zone-plate antenna without the reflector and $\lambda/4$ spacer was investigated. The gain of the antenna with nothing behind the zone plate was found to approach that of the fully configured antenna with the $\lambda/4$ spacer and reflector. The reflection from the open rings (dielectric-air interface) which is responsible for this phenomena is enhanced as the dielectric constant of the

substrate is increased. Thus on substrates with high permittivity, such as alumina and gallium arsenide, the reflector and $\lambda/4$ spacer may not be necessary.

ACKNOWLEDGMENT

The authors would like to thank James Wiltse and the late James Gallagher of the Georgia Tech Research Institute for continued interest in and support of this work.

REFERENCES

[1] D. M. Pozar, "Considerations for millimeter wave printed antennas," *IEEE Trans. Antennas Propagat.*, vol. AP-31, pp. 740–747, Sept. 1983.

[2] N. G. Alexopoulos, P. B. Katehi, and D. B. Rutledge, "Substrate optimization for integrated circuit antennas," *IEEE Trans. Microwave Theory Tech.*, vol. MTT-31, pp. 550–557, July 1983.

[3] D. B. Rutledge, D. P. Neikirk, and D. P. Kasilingam, "Integrated-circuit antennas," *Infrared and Millimeter Waves*, vol. 10, pp. 1–90, 1983.

[4] D. B. Rutledge and M. S. Muha, "Imaging antenna arrays," *IEEE Trans. Antennas Propagat.*, vol. AP-30, pp. 535–540, July 1982.

[5] D. P. Neikirk, "Integrated detector arrays for high resolution far-infrared imaging," Ph.D. dissertation, California Inst. Tech., 1984.

[6] P. P. Tong, "Millimeter-wave integrated-circuit antenna arrays," Ph.D. dissertation, California Inst. Tech., ch. 3, 1985.

[7] K. Lee and M. Frerking, "Planar antennas on thick dielectric substrates," in *Proc. 12th Int. Conf. Infrared Millimeter Waves*, Lake Buena Vista, FL, Dec. 1987, pp. 216–217.

[8] R. C. Compton, R. C. McPhedran, Z. Popović, G. M. Rebeiz, P. P. Tong, and D. B. Rutledge, "Bow-tie antennas on a dielectric half-space: Theory and experiment," *IEEE Trans. Antennas Propagat.*, vol. AP-35, pp. 622–631, June 1987.

[9] P. H. Siegel and R. J. Dengler, "The dielectric-filled parabola: a new millimeter/submillimeter wavelength receiver/transmitter front end," *IEEE Trans. Antennas Propagat.*, vol. 39, pp. 40–47, Jan. 1991.

[10] G. M. Rebeiz, W. G. Regehr, D. B. Rutledge, R. L. Savage and N. C. Luhmann, "Submillimeter-wave antennas on thin membranes," *Int. J. Infrared and Millimeter Waves*, vol. 8, pp. 1249–1255, Oct. 1987.

[11] G. M. Rebeiz, D. P. Kasilingam, Y. Guo, P. A. Stimson, and D. B. Rutledge, "Monolithic millimeter-wave two dimensional horn imaging arrays," *IEEE Trans. Antennas Propagat.*, vol. 38, pp. 1473–1482, Sept. 1990.

[12] L. F. Van Buskirk and C. E. Hendix, "The zone plate as a radio-frequency focusing element," *IRE Trans. Antennas Propagat.*, vol. AP-9, pp. 319–320, May 1961.

[13] J. E. Garrett and J. C. Wiltse, "Fresnel zone plate antennas at millimeter wavelengths," *Int. J. Infrared and Millimeter Waves*, vol. 12, pp. 195–220, Mar. 1991.

[14] G. S. Smith, "Directive properties of antennas for transmission into a material half-space," *IEEE Trans. Antennas Propagat.*, vol. AP-32, pp. 232–246, Mar. 1984.

[15] M. Kominami, D. M. Pozar, and D. H. Shaubert, "Dipole and slot elements and arrays on semi-infinite substrates," *IEEE Trans. Antennas Propagat.*, vol. AP-33, pp. 600–607, June 1985.

[16] M. A. Gouker, "Studies of dipole antennas on finite thickness substrates with planar integrated focusing elements," Ph.D. dissertation, Georgia Inst. Tech., Atlanta, GA, May 1991.

[17] M. A. Gouker and G. S. Smith, "Measurements of strip dipole antennas on finite thickness substrates at 230 GHz," to be published in *IEEE Microwave Guided Wave Lett.*, vol. 2, pp. 79–81, Feb. 1992.

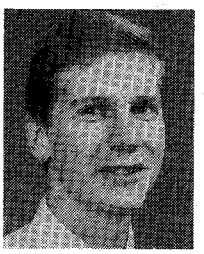

Mark A. Gouker (S'84) was born in Rockville, MD on December 29, 1961. He received the B.S. degree in physics from Emory University, Atlanta, GA in 1983, and the M.S. and Ph.D. degrees from the Georgia Institute of Technology in 1985 and 1991, respectively.

He was a Research Engineer at the Georgia Tech Research Institute from 1985 to 1987, and a Graduate Research Assistant at the Georgia Tech Research Institute from 1988 to 1991. He is currently with the MIT Lincoln Laboratory in Lexington MA. His research interests are in millimeter-wave integrated circuits and antennas.

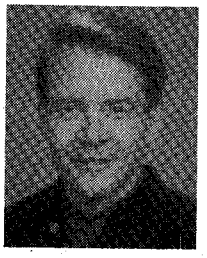

Glenn S. Smith (S'65–M'72–SM'80–F'86) was born in Salem, MA, on June 1, 1945. He received the B.S.E.E. degree from Tufts University, Medford, MA, in 1967 and the S.M. and Ph.D. degrees in applied physics from Harvard University, Cambridge, MA, in 1968 and 1972, respectively.

From 1972 to 1975 he served as a Postdoctoral Research Fellow at Harvard University and also as a part-time Research Associate and Instructor at Northeastern University, Boston, MA. In 1975, he joined the faculty of the Georgia Institute of Technology, Atlanta, GA, where he is currently Regents' Professor of Electrical Engineering.

Dr. Smith is co-author of the book, *Antennas in Matter: Fundamentals, Theory and Applications.*